An analytical method to evaluate the capacity of laterally loaded piles in unsaturated soils

Leonardo Maria Lalicata[1] , *Agostino Walter* Bruno[1] and *Domenico* Gallipoli[1]

[1]Department of Civil, Chemical and Environmental Engineering, University of Genoa, 16145 Genoa, Italy

Abstract. The growing pressures of climate change, increased usage and unprecedented geo-hazards impose a modification in the way civil engineering structures are designed and constructed. This is particularly true for geotechnical works, which are very sensitive to changes of environmental conditions. For instance, the response of a pile under lateral loading is strongly influenced by the stiffness and strength of the first few metres of soil below the surface, which are often partly saturated. To consider this effect, the present paper describes an analytical method, which extends the well-known Broms approach to predict the lateral capacity of piles in unsaturated soils. More specifically, the proposed method considers the combined effects of the position of the ground water table and the extra strength of the partially saturated soil above it. Compared to Broms approach, the solution introduces four additional non-dimensional parameters that relate the soil-water retention behaviour to the geometry of the pile. The method provides a direct evaluation of the lateral pile capacity in partly saturated soils, which can be used as a basis for more accurate design.

1 Introduction

Pile foundations are frequently chosen in geotechnical design to support a combination of axial forces, lateral forces and concentrated moments. Consideration of lateral forces is crucial, for example, in the design of tall buildings, bridge abutments, earth-retaining structures and wind turbines. Experimental, analytical and numerical studies show that the response of flexible piles is largely influenced by the pile-soil stiffness ratio whereas, for short and rigid piles, the behaviour is governed by both stiffness and slenderness ratio [1]. The non-linear soil behaviour also strongly influences design parameters such as head displacement, maximum bending moment and critical length.

The kinematics of pile foundations under lateral loading may affect a significant volume of soil several diameters below ground level. In many applications, most of the interested soil lies above the ground water table (GWT) and is therefore partly saturated. Although traditional methods for the design of laterally loaded piles assume that the soil is either dry or fully saturated, the effect of partial saturation is lately attracting fresh research interest [2-6]. Recently, Lalicata *et al.* [7] extended the well-known Broms method for dry or saturated soils to unsaturated soils by taking into account the combined effects of the position of the GWT and the cohesion of the unsaturated soil above it.

In this paper, the main features of the method by Lalicata *et al.* [7] are briefly recalled and the influence of the soil-water retention parameters on the computed pile capacity are highlighted before validating results against field data.

2 Shear strength in unsaturated soils

The soil above the ground water table (GWT) is often unsaturated with pores partly filled by air and partly filled by water. The difference between pore air and water pressures, $s = u_a - u_w$ is named matric suction or, simply, suction (as in the following part of this paper). In most applications, the pore air pressure is atmospheric (i.e. equal to zero) while the pore water pressure is tensile (i.e. negative), meaning that the suction is equal to the pore water pressure changed of sign.

The increase in soil strength generated by capillarity above the GWT is modelled through the introduction of an extra cohesion, which is named "apparent cohesion" [8]. The apparent cohesion is often calculated by the expression $S_r s \tan\varphi$ where S_r is the degree of saturation and φ is the friction angle of the soil. The above expression of apparent cohesion is obtained from the Mohr-Coulomb failure criterion written in terms of Bishop stress [9] with $\chi = S_r$ as:

$$\tau_f = c + (\sigma + S_r s)\tan\varphi = c + \sigma\tan\varphi + S_r s\tan\varphi \qquad (1)$$

where c is the effective cohesion and $\sigma\tan\varphi$ is the frictional strength which depends on total stresses. In eq. (1) the apparent cohesion $S_r s\tan\varphi$ can be expressed in terms of the suction s via the Soil Water Retention Curve (SWRC), which is a material law linking the degree of saturation S_r of the soil to the suction s.

Among the many SWRCs proposed in the literature, the following Van Genuchten [10] equation has been chosen in this study:

$$S_r = S_{r,res} + \left(1 - S_{r,res}\right)\left(1 + \left(\frac{s}{s^e}\right)^n\right)^{-m} \quad (2)$$

where $S_{r,res}$ is the residual degree of saturation and s^e (kPa) approximates the air entry suction. Note that Lalicata *et al.* [7] assumed $S_{r,res}$ equal to zero for sake of simplicity. The present work instead considers SWRCs of three real soils that may exhibit a non-null residual degree of saturation (see Section 5). The air entry suction also coincides with the air expulsion suction due to the uniqueness of the relationship between degree of saturation and suction. The non-dimensional parameters n and m control the shape of the SWRC curve where, to simplify calibration, m is related to n by the relationship $m = 1 - \frac{1}{n}$.

3 Extension of Broms method to unsaturated soils

Broms [11, 12] provides the lateral pile capacity and the corresponding maximum bending moment as a function of: i) the pile geometry, i.e. the length L and load eccentricity e, ii) the pile yielding moment of the pile M_y iii) the soil resistance, i.e. the friction angle φ or undrained shear strength s_u and iv) the type of failure, i.e. short, intermediate, or long pile failure mechanism. In the short pile mechanism, only the ultimate soil resistance is attained, and the pile reacts with its whole length.

Conversely, in the case of intermediate or long pile mechanisms, both the soil and pile ultimate resistance are mobilised. The pile resistance is attained in one or two cross-sections depending on both the head restraint and the specific failure mechanism. This corresponds to the formation of one or two plastic hinges at the ground surface and/or at some depth below it. In the presence of a buried plastic hinge, the pile reacts only with the section comprised between the ground surface and the plastic hinge. Both pile and soil are assumed rigid-perfectly plastic so that, once the limit soil resistance p_{lim} and pile yielding moment M_y are defined, the solution can be found by imposing the translational and rotational equilibrium.

Broms solution was derived for either purely frictional (Fig. 1a) or purely cohesive (Fig. 1b) soils. Conversely, a cohesive-frictional soil is here considered due to the apparent cohesion generated by the suction above the GWT. Note also that, for simplicity, the effective cohesion c of eq. (2) is taken equal to zero.

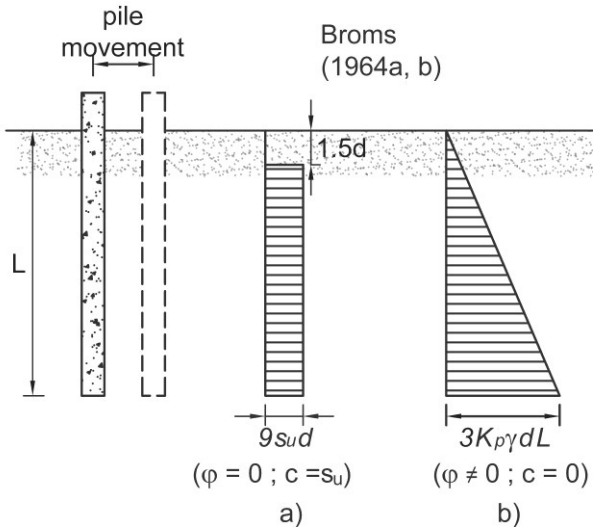

Fig. 1. Soil resistance profiles for a) purely cohesive soil according to Broms [11]; b) purely frictional soil according to Broms [12].

3.1 Including apparent cohesion into Broms method

The pore water pressure profile, and hence the suction profile, above the GWT depends on the hydraulic boundary conditions at the ground surface (Fig. 2). Once the soil-water retention properties of eq. (2) and the suction profile are known, the apparent cohesion profile $S_r s \tan\varphi$ is readily calculated as shown in Fig. 2c and 2d.

To solve analytically the translational and rotational equilibrium, the apparent cohesion profile is here idealised by a simpler design profile, e.g. a constant or triangular design profile, having the same integral area of the actual one (Fig. 2c and 2d).

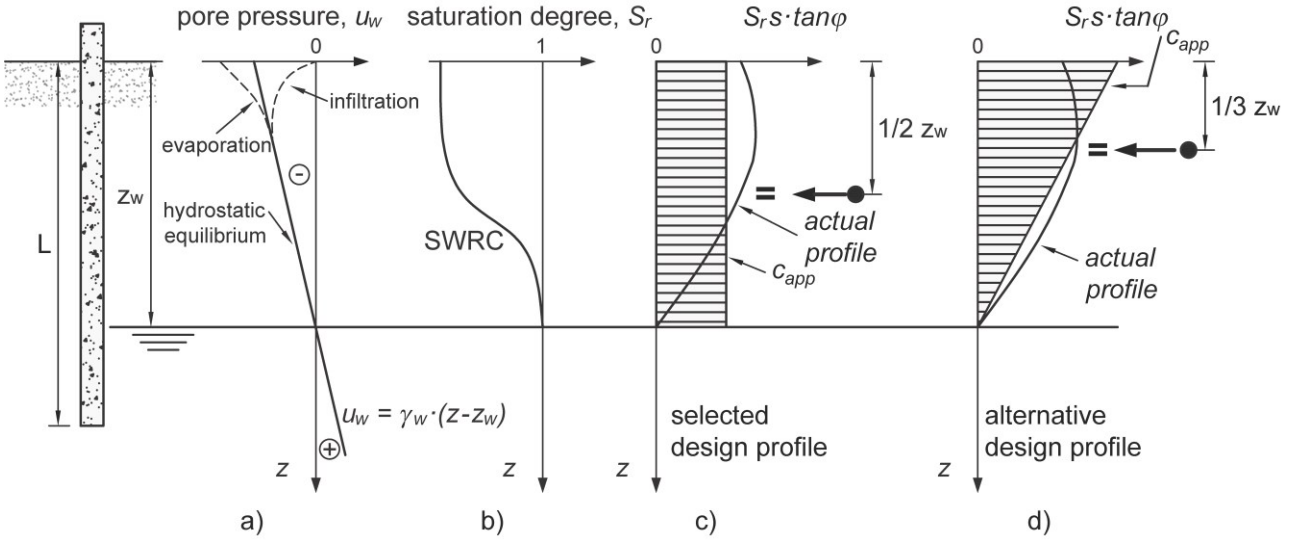

Fig. 2. Evaluation of apparent cohesion above the GWT (modified from [7]).

The equivalence of integral areas ensures that the soil resisting force is correctly calculated by the design profile, though the corresponding lever arm is likely to differ from the actual one.

Both constant and triangular design profiles of Fig. 2c and 2d therefore respect the translational equilibrium but they do not necessarily respect the rotational equilibrium.

The triangular design profile (Fig. 2d) has the advantage of correctly calculating a zero apparent cohesion in correspondence of the GWT, where suction reduces to zero. Conversely, the constant design profile (Fig. 2c) has the advantage of being more conservative as the lever arm of the resulting force, with respect to the ground surface, is bigger and therefore produces smaller values of lateral pile capacity than the triangular one.

Thus, in the interest of safety, only the constant design profile is considered hereafter. The constant design apparent cohesion c_{app} is calculated as the average of the $S_r s \tan\varphi$ profile over the reacting unsaturated depth L_u as:

$$c_{app} = \frac{\int_0^{L_u} (S_r s \tan\varphi) dz}{L_u} \quad (3)$$

The reacting unsaturated depth L_u coincides with the GWT depth if the failure mechanism extends below the unsaturated layer while it is smaller than the GWT depth if the failure mechanism is strictly contained within the unsaturated layer. This latter circumstance happens when the pile is shorter than the depth of the GWT or if plastic hinges form above the GWT.

Under the hypothesis of drained soil response, the soil reaction p_{lim} is calculated above and below the GWT as:

$$p_{lim} = \left(3K_p\,\gamma\,z + 9\sqrt{K_p}\,c_{app}\right) d \qquad for\ z < z_w \quad (4a)$$

$$p_{lim} = \left(3K_p\,\gamma\,z_w + 3K_p\,\gamma'(z - z_w)\right) d \qquad for\ z > z_w \quad (4b)$$

where z_w is the GWT depth, d is the pile diameter, γ is the soil bulk unit weight, $\gamma' = \gamma - \gamma_w$ is the soil submerged unit weight (where γ_w is the water unit weight) and $3K_p = 3\tan^2\left(45° + \frac{\varphi}{2}\right)$ is the passive earth pressure coefficient where the factor of 3 accounts for three-dimensional effects. Following Cecconi *et al.* [13], the three-dimensional passive earth pressure coefficient for the cohesive term is taken equal to $9\sqrt{K_p}$.

Inspection of eq. (4) indicates that: i) the apparent cohesion c_{app} only contributes to the strength of the top unsaturated layer and ii) the frictional term depends on the bulk unit weight γ in the top unsaturated layer and on the submerged unit weight $\gamma' = \gamma - \gamma_w$ in the bottom saturated layer. In the sake of simplicity, the bulk unit weight γ is here assumed to be identical in both unsaturated and saturated layers. The solution of the translational and rotational equilibrium is presented by Lalicata *et al.* [7] in a dimensionless form that provides the horizontal capacity H_{lim} and the corresponding maximum bending moment M_{lim} in terms of the non-dimensional groups listed in Table 1. Compared to Broms, the solution includes additional non-dimensional groups linked to the GWT depth and the SWRC parameters.

More specifically, the apparent cohesion is taken into account through the non-dimensional group C, which is defined in terms of c_{app} as shown in Table 1. It can be further shown that the value of c_{app} in eq. (4) depends on the non-dimensional GWT depth z_w/d, air entry suction $s^e/\gamma d$, unit weight of water γ_w/γ, slope of the SWRC n, residual degree of saturation $S_{r,res}$ and friction angle φ (see Lalicata *et al.* [7] for further details). Interestingly, the non-dimensional group $s^e/\gamma d$ indicates that, for a given soil and GWT depth, the effect of the air entry suction on the pile horizontal capacity decreases with increasing values of the pile diameter.

Table 1. Non-dimensional groups.

Geometry	Slenderness	$\frac{L}{d}$
	Eccentricity	$\frac{e}{d}$
Load and moment	Limit load	$\frac{H_{lim}}{K_p\,\gamma\,d^3}$
	Limit moment	$\frac{M_{lim}}{K_p\,\gamma\,d^4}$
	Yielding moment	$\frac{M_y}{K_p\,\gamma\,d^4}$
GWT	Submerged soil unit weight	$\frac{\gamma'}{\gamma}$
	Water unit weight	$\frac{\gamma_w}{\gamma}$
	Water table depth	$\frac{z_w}{d}$
SWRC	Cohesive term	$C = \frac{9\sqrt{K_p}}{K_p}\frac{c_{app}}{\gamma\,d}$
	Air entry value of suction	$\frac{s^e}{\gamma\,d}$
	Slope of SWRC	n
	Residual degree of saturation	$S_{r,res}$

4 Validation against field data

The proposed method has been validated against field tests on free head short rigid piles embedded in three distinct unsaturated soils, i.e. a weathered granite [14], a sand with clay and silt [15] and a fine sand [16], . In all cases, the water table was deeper than the toe of the pile ($z_w > L$) so that the unsaturated reacting depth coincides with the pile length (i.e. $L_u = L$). The authors of the above testing campaigns also reported the average degree of saturation along the pile length as obtained from site investigations. Due to the small dimensions of the piles

and the deep GWT, the degree of saturation can be assumed constant along the pile length and equal to the average value. The corresponding suction was then computed according to the SWRCs declared by the above authors. Finally, the apparent cohesion $S_r s \tan\varphi$ was obtained from the corresponding values of degree of saturation and suction, thus assuming a constant design profile as shown in Fig. 2c.

The material and geometrical parameters of the testing campaigns are summarised in Table 2. Calibration details are reported in both the original publications [14-16] and in Lalicata *et al.* [7].

The lateral capacity of free head short piles is computed by using eq. (5a) and imposing the rotational equilibrium around the pile toe as:

$$H_{lim} \cdot (e + L) = 3K_p \gamma d L \cdot \frac{L}{2} \cdot \frac{L}{3} + 9\sqrt{K_p} c_{app} d L \cdot \frac{L}{2} \qquad (5a)$$

or in non-dimensional form:

$$\frac{H_{lim}}{K_p \gamma d} = \left(\frac{1}{2}\left(\frac{L}{d}\right)^3 + \frac{1}{2} C \left(\frac{L}{d}\right)^2\right) \cdot \frac{1}{\left(\frac{e}{d} + \frac{L}{d}\right)} \qquad (5b)$$

where the non-dimensional group C is defined in Table 1. Compared to Broms solution for purely frictional soils, eq. (5b) incorporates the additional term $\frac{1}{2} C \left(\frac{L}{d}\right)^2$ that accounts for the extra cohesive strength of the unsaturated soil layer.

Fig. 3 compares the measured and predicted values of lateral capacity showing that the proposed method captures well the experimental data, particularly those by Truong [15]. In this case, the good estimate of the lateral pile capacity relies on the accurate measurement of the soil-water retention behaviour. Conversely, a higher discrepancy (>20%) between measured and predicted values is observed for two of the three piles tested by Choi *et al.* [14]. This difference may be due to the lack of information about the variation of suction with depth, which was not provided by the authors. Inspection of Fig. 3 confirms that accounting for the extra soil strength due to partial saturation leads to a more accurate estimate of the lateral pile capacity compared with Broms solution, which underestimates all experimental data.

Equation (5b) highlights the effect of the non-dimensional cohesive group C on the lateral capacity of piles. It is worth noting that even a small amount of apparent cohesion may significantly increase the lateral pile capacity. With reference to the tests of Choi *et al.* [14] and Wang *et al.* [16], the apparent cohesion is relatively low (it ranges from 2.34 to 10.9), but its effect on the predicted lateral capacity of the pile is very evident in Fig. 3. In the tests from Choi *et al.* [14], the non-dimensional cohesive group C is responsible for 40% to 72% of the pile capacity depending on the value of L/d while in the test from Wang *et al.* [16] it accounts for 35% to 87% of the pile capacity.

Table 2. Material and geometrical parameters of laterally loaded pile tests.

Reference	L/d (-)	e/d (-)	γ (kN/m³)	φ (°)	c_{app} (kPa)
Choi *et al.* [14] d = 0.4m	3.0	5.0	18	30	10.9
	6.0	5.0			5.46
	6.0	0.4			
Truong [15] d = 0.127m	10.9	2.0	17.5	35	33.2
	11.1	2.0			
	10.6	1.7			
	11.7	2.0			
Wang *et al.* [16] d = 0.273m	3.7	1.2	16.4	38	2.34
	3.7	1.2			
	5.5	1.3			
Wang *et al.* [16] d = 0.457m	2.2	0.7			
	2.2	0.8			
	3.3	0.7			

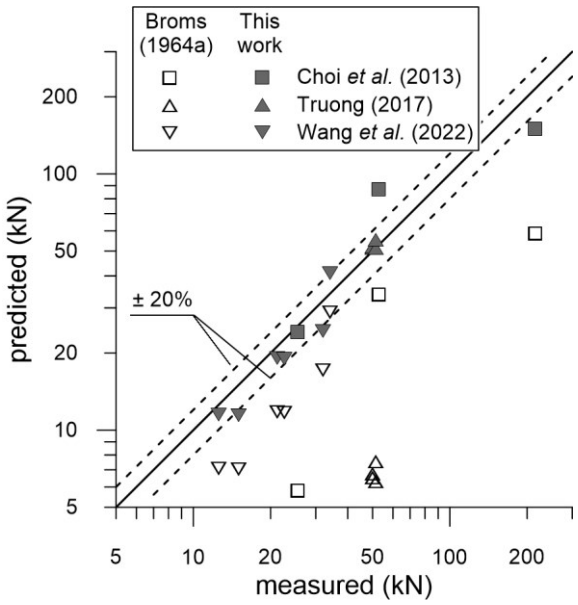

Fig. 3. Comparison between measured and predicted values of lateral pile capacity.

5 Influence of partial saturation on the lateral pile capacity

The importance of the soil-water retention properties is here explored for the common case of restrained head pile. For the sake of brevity, the analysis is restricted to the case of short pile, i.e. the case where the pile yielding moment is always larger than the maximum bending moment. The interested reader can find the general solution in Lalicata *et al.* [7].

As shown in Fig. 4, the failure mechanism of a short restrained head pile is a rigid horizontal translation that involves the whole pile length and the maximum bending moment is therefore located at the pile head.

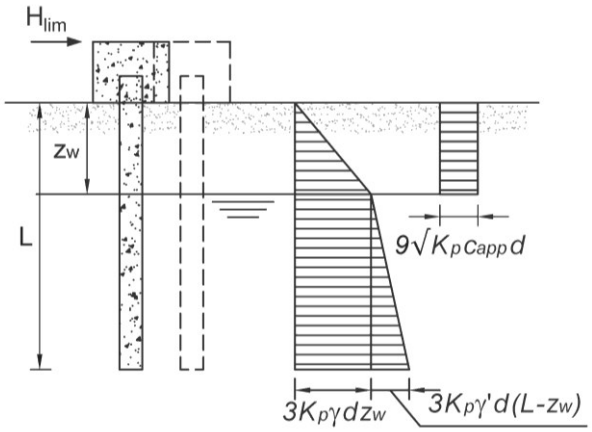

Fig. 4. Restrained head pile: failure mechanism and soil resistance profiles for the case of short pile.

The non-dimensional lateral capacity of the pile is computed from the horizontal equilibrium and is given by eqs. (6a) and (6b) when $L > z_w$ and $L \leq z_w$, respectively:

$$\frac{H_{lim}}{K_p \gamma d^3} = \left[\frac{3}{2}\left(\frac{z_w}{d}\right)^2 + 3\frac{z_w}{d}\left(\frac{L}{d} - \frac{z_w}{d}\right) + \frac{3}{2}\frac{\gamma'}{\gamma}\left(\frac{L}{d} - \frac{z_w}{d}\right)^2\right] + C\frac{z_w}{d} \quad (6a)$$

$$\frac{H_{lim}}{K_p \gamma d^3} = \frac{3}{2}\left(\frac{L}{d}\right)^2 + C\frac{L}{d} \quad (6b)$$

Eqs. (6a) and (6b) indicate that the horizontal capacity depends on the geometrical parameters L/d, e/d and z_w/d, on the normalised bulk unit weight of the soil γ'/γ and on the SWRC properties via the parameter C. In detail, the first term on the right and side of eqs. (6a) and (6b) describes the contribution of the frictional strength while the second term relates to the cohesive strength of the unsaturated layer above the GWT.

It is worth noting that, since the lateral capacity is evaluated by imposing the horizontal equilibrium, eqs. (6a) and (6b) are rigorously true because their unsaturated cohesive terms (i.e. $C\frac{z_w}{d}$ and $C\frac{L}{d}$, respectively) coincide with those calculated via the integration of the apparent cohesion profile $S_r s \tan\varphi$.

To better illustrate the importance of accounting for the apparent cohesion of the unsaturated layer, eqs. (7a) and (7b) are applied to the prediction of the lateral capacity of a 0.4 m diameter pile having an embedded length of 6m, i.e. a slenderness ratio $L/d = 15$. The retention parameters of three real soils are considered, namely a fine silt (B-grade kaolin clay [17]), a silty sand (Jossigny Silt [18]) and a sand with clay (Rudlingen sand [19]). To simplify comparison, the bulk unit weight of the soil and the friction angle have been assumed identical in all cases and equal to γ = 18 kN/m^3 and φ = 28°, respectively (i.e. K_p = 2.77). The unit weight of water is γ_w = 10kN/m^3 while the depth of the the GWT ranges between 0 (fully saturated conditions) and 12 m, so that z_w/d spans from 0 to 30. The pore pressure profile is assumed hydrostatic above and below the GWT, i.e. $u_w = \gamma_w(z - z_w)$.

The calibration of the Van Genuchten SWRC against experimental data is illustrated in Fig. 5 while the corresponding parameters are listed in Table 3.

Table 3. Parameter values of Van Genuchten SWRC.

Material	s^e (kPa)	n (-)	$S_{r,res}$ (-)	$s^e/\gamma d$
B-grade kaolin clay [17]	58.0	1.37	0	8.06
Jossigny Silt [18]	8.0	1.27	0	1.11
Rudlingen sand [19]	1.2	1.88	0.41	0.17

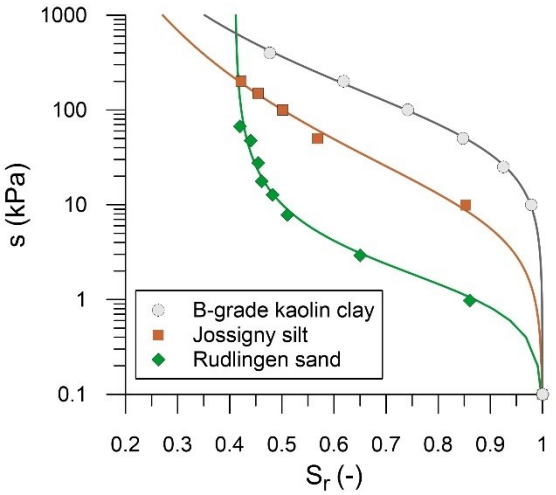

Fig. 5. Interpolation of experimental data by Van Genuchten SWRC.

Fig. 6 shows the lateral pile capacity computed by the present work and Broms solution for different values of z_w/d from full soil saturation (z_w/d = 0) to a GWT depth well below the pile toe (z_w/d = 15). The solution for C = 0 corresponds to the assumption of a dry soil above the GWT. Inspection of Fig. 6 indicates that, for shallow GWT depths (i.e. small values of z_w/d), the present work calculates smaller values of the lateral pile capacity compared to Broms dry soil solution.

However, as the GWT deepens and the resisting contribution of c_{app} grows larger, the trend reverses and the present work provides larger values of the lateral pile capacity compared to Broms dry soil solution. Over this range, low values of $s^e/\gamma d$ and large values of n reduce the increase of lateral pile capacity predicted by the present method compared to Broms dry soil solution. For the Rudlingen sand, however, this effect is partly counteracted by the high residual degree of saturation (Table 3). Even for the relatively low value of $s^e/\gamma d$ = 0.17 of Rudlingen sand, the non-dimensional lateral capacity predicted by the present method is larger than Broms dry soil solution by 4.7% at z_w/d = 10 and by 23% at z_w/d = 15.

Finally, the z_w/d threshold marking the transition from smaller to larger predictions of lateral pile capacity compared to Broms dry soil solution depends on the SWRC properties (i.e. on the values of $s^e/\gamma d$, n and $S_{r,res}$).

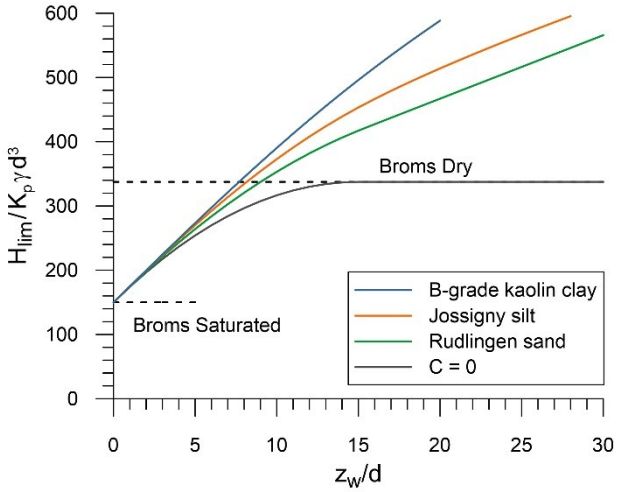

Fig. 6. Predicted non-dimensional lateral pile capacity as a function of GWT depth.

6 Conclusions

Broms method for the calculation of the horizontal pile capacity has been extended to include the presence of a groundwater table (GWT) and the cohesive strength of the unsaturated layer above it. Above the GWT, the soil resistance is given by two components: a frictional term, which depends on the total stress, and a cohesive term (apparent cohesion), which depends on the soil-water retention properties. To allow a closed-form solution, the apparent cohesion has here been assumed constant and equal to the average value of the actual apparent cohesion profile above the GWT.

The method has been successfully validated against the values of the lateral capacity of piles as measured in works published in literature. Results confirm that neglecting the partially saturated state of the soil above the GWT leads to a significant underestimation of the lateral pile capacity.

In the present solution, additional non-dimensional groups have been introduced to represent the influence of unsaturated conditions, i.e. the normalised GWT depth z_w/d, the slope of the soil-water retention curve n, the residual degree of saturation $S_{r,res}$ and the normalised air entry value of suction $s^e/\gamma d$ (linking the air entry value of suction to the vertical stress at one diameter of depth).

The effect of apparent cohesion increases with growing values of $s^e/\gamma d$ and $S_{r,res}$ while decreases with growing values of n. For reasonably low values of n, even the apparent cohesion of an unsaturated sandy soil can provide a significant increase in horizontal capacity (20 – 40%) for $z_w/d > 15$ compared to Broms dry soil solution.

The present method provides an expeditious, and yet effective, estimation of the influence of partial saturation on the capacity of laterally loaded piles. It is hoped that this method could serve as a basis to further disseminate the application of unsaturated soils mechanics principles among engineering practitioners.

References

1. L.M. Lalicata, G. M. Rotisciani, A. Desideri, F. Casini. Geosc. ***12***(1), 1 (2021) https://doi.org/10.3390/geosciences12010001
2. L.M. Lalicata, A. Desideri, F. Casini, L. Thorel. *Can. Geotech. J.* ***56***(11), 1545–1556 (2019) https://doi.org/10.1139/cgj-2018-0322
3. X. Cheng, S.K. Vanapalli. Comp. Geotech. 140, 104480 (2021) https://doi.org/10.1016/j.compgeo.2021.104480
4. M. Ghazavi, E. Mahmoodi, H. El Naggar. A. Geo. 17 (2022) http://dx.doi.org/10.1007/s11440-022-01647-w
5. L.M. Lalicata, G. M. Rotisciani, A. Desideri, F. Casini, L. Thorel. In: *Geotechnical Research for Land Protection and Development. CNRIG 2019, Lecture Notes in Civil Engineering*, Springer, Cham, 40, 713-722 (2019) https://doi.org/10.1007/s11440-022-01532-6
6. X. Zou, Z. Yang, W. Wu. S. Dyn. Earthquake Eng. 165, 107672 (2023) http://dx.doi.org/10.1016/j.soildyn.2022.107672
7. L.M. Lalicata, A.W. Bruno, D. Gallipoli. Comp. Geotech. **155** (2023) https://doi.org/10.1016/j.compgeo.2022.105189
8. S.K. Vanapalli, D.G. Fredlund, D.E. Pufahl, A.W. Clifton. Can. Geotech. J. **33**, 3, 379–392. (1996) https://doi.org/10.1139/t96-060.
9. A. W. Bishop, G. E. Blight. Géotechnique ***13***, 3, 177–197 (1963) https://doi.org/10.1680/geot.1963.13.3.177
10. M.Th. van Genuchten. S. Sc. Soc. Am. J. **44**, 5, 892–898 (1980). https://doi.org/10.2136/sssaj1980.03615995004400050002x
11. B. B. Broms. J. Soil Mech. Found. Div. ***90***, 3, 123-156 (1964)
12. B. B. Broms. J. S. Mech. Found. Div. ***90***, 2, 27-63 (1964)
13. M. Cecconi, V. Pane, A. Vecchietti, D. Bellavita. Soils Found. **59**, 4, 840–856 (2019) https://doi.org/10.1016/j.sandf.2019.01.007
14. H.Y. Choi, S.R. Lee, H.I. Park, D.H. Kim. (2013). J. Geotech. and Geoenv. Eng. **139**(9), 1477–1489. https://doi.org/10.1061/(ASCE)GT.1943-5606.0000831
15. P. Truong. *Experimental investigation on the behaviour of laterally loaded piles in soft clay, sand and residual soils*. PhD thesis. (2017)
16. H. Wang, B. M. Lehane, M.F. Bransby, L.Z. Wang, Y. Hong. *A. Geo.* 1-12. (2022)
17. L.M. Lalicata, G. M. Rotisciani, A. Desideri, F. Casini, L. Thorel. In: *Eu. Conf. Unsat. Soils*. E3S Web of Conferences, 2020, 195, 02012 10.1051/e3sconf/202019502012
18. G.M. Rotisciani, G. Sciarra, F. Casini, A. Desideri. Int. J. Num. An. Meth. Geomech. **39**, 11, 1212-1234 (2015) http://dx.doi.org/10.1002/nag.2359
19. P. Sitarenios, F. Casini, A. Askarinejad, S. Springman. Géotechnique ***71***, 2, 96–109 (2019) https://doi.org/10.1680/jgeot.18.P.188